Inorg. Chem. **2009**, *48*, 3628−3638

What Singles out the FeO^{2+} Moiety? A Density-Functional Theory Study of the Methane-to-Methanol Reaction Catalyzed by the First Row Transition-Metal Oxide Dications $MO(H_2O)_p^{2+}$, M = V−Cu

Carine Michel and Evert Jan Baerends*

Theoretische Chemie, Vrije Universiteit Amsterdam, De Boelelaan 1083, 1081 HV Amsterdam, The Netherlands

Received November 1, 2008

Metaloxo species are often postulated as key active species in oxidative catalysis. Among all, the quintet FeO^{2+} moiety is particularly widespread and active: aliphatic C−H bonds undergo hydroxylation easily through a H-abstraction/O-rebound mechanism. The high electrophilicity of quintet FeO^{2+} originates from its electronic structure: a low lying vacant σ^* can accept electronic density from the aliphatic C−H bond. What singles out this quintet FeO^{2+}? Its lowest vacant acceptor orbital energy? its shape (σ^* vs π^*)? or has its biological importance more simply arisen from the high iron abundance? To answer those questions, we have performed density-functional theory calculations to study systematically the methane-to-methanol reaction catalyzed by $MO(H_2O)_p^{2+}$ complexes (M = V, Cr, Mn, Fe, Co, $p = 5$ and M = Ni, Cu, $p = 4$) in gas phase. We show here that the lower the MO^{2+} acceptor orbital lies in energy, the lower the H-abstraction barrier is in general. However, a σ^* acceptor orbital is much more efficient than a π^* acceptor orbital for a given energy. Finally, we found that indeed, the FeO^{2+} moiety is particularly efficient but also CoO^{2+} and MnO^{2+} could be good candidates to perform C−H hydroxylation.

Introduction

Homogeneous catalytic oxidation processes have attracted much attention for years for several reasons:[1] (1) they are one of the most challenging processes to bring to satisfactory peformance (yield, selectivities, sustainability, etc.); (2) the existing processes often leave room for considerable improvement; (3) involved mechanisms are quite complex (multiple pathways, multiple spin states); (4) they have extensive applications in various areas from fine chemical production[2] to waste degradation or bleaching.[3]

Currently, the main challenge is the development of green oxidative processes. To reach this goal, the stoichiometric oxidant has to be efficient, benign, and easily accessible. Dioxygen from air or hydrogen peroxide are the favorite ones, but they cannot oxidize directly and selectively alkanes into more valuable functionalized products such as alcohols, esters, aldehydes, ketones, and others.[1,4] Among all, the selective conversion of methane into various oxidized products, such as methanol and acetic acid, is particularly challenging: methane is the most abundant and unreactive hydrocarbon, a cheap raw material, and a greenhouse gas. New mild green selective routes to convert methane into valuable products could contribute to sustainable routes to methanol or other oxidized products and also to methods to lower its present concentration in the atmosphere. A widely used strategy in this field is to use transition metal complexes as catalysts together with a stoichiometric oxidant, such as dioxygen or peroxides. For instance, iron derivatives are used in Fenton-like processes in bleaching.[5,6] Manganese is a well-known key ingredient of the Jacobsen−Katsuki catalyst to perform alkene epoxidation.[7] And now, (salen)manganese complexes can also perform asymmetric oxidation of the σ C−H bond.[8] Last but not least, vanadium complexes such

* To whom correspondence should be addressed. E-mail: ej.baerends@few.vu.nl.

(1) Barton, D.; Martell, A.; Sawyer, D.; Sheldon, R.; van Santen, R. *Catalytic Oxidation: Principles and Applications*; World Scientific: Singapore, 1995.
(2) Caron, S.; Dugger, R. W.; Gut Ruggeri, S.; Ragan, J. A.; Brown Ripin, D. H. *Chem. Rev.* **2006**, *106*, 2943–2989.
(3) Hage, R.; Lienke, A. *Angew. Chem., Int. Ed.* **2006**, *45*, 206–222.
(4) Simandi, L. *Catalytic Activation of Dioxygen by Metal Complexes*; Kluwer Academic Publishers: Dordrecht, 1992.
(5) Fenton, H. J. H. *Chem. News* **1876**, 190.
(6) Pignatello, J. J.; Oliveros, E.; MacKay, A. *Crit. Rev. Environ. Sci. Technol.* **2006**, *36*, 1–84.
(7) Katsuki, T. *Coord. Chem. Rev.* **1995**, *140*, 189–214.
(8) Katsuki, T. *Synlett* **2003**, *3*, 281–297.

10.1021/ic802095m CCC: $40.75
Published on Web 03/20/2009

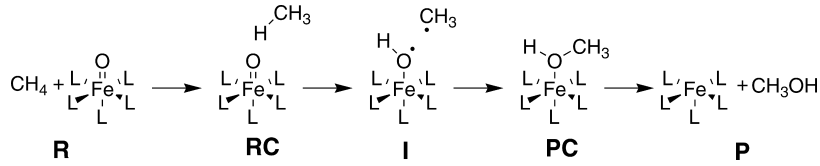

Figure 1. H-abstraction/O-rebound mechanism scheme. **R** is the reactants. **RC** is the reactants complex. **I** is the intermediate. **PC** is the products complex. **P** is the products.

as amadavine derivatives can perform a single-pot conversion of methane into acetic acid in the presence of potassium peroxodisulphate ($K_2S_2O_8$).[9−11] In all those examples, the postulated active species is the MO^{n+} moiety: FeO^{2+} in Fenton-like processes, MnO^{3+} in Jacobsen−Katsuki epoxidation,[12] VO^{2+} in amadavine derivatives.

The most widely spread MO^{n+} moiety is the oxoiron(IV) (ferryl ion) FeO^{2+}, well established in hydroxylating aliphatic C−H bonds.[13] A well-known example is the active center in heme iron enzymes such as cytochrome P450.[14−17] There is also evidence of such a reactive moiety for some non-heme enzymes,[18,19] for iron containing zeolites,[20,21] for biomimetic complexes,[22] or for the Fenton reaction.[23−25] This noticeable wide range of use, from enzymes to zeolite catalysts, leads us to the following question: What singles out FeO^{2+}?

First of all, iron is the most abundant transition metal in the Earth's crust, easily accessible and cheap.[26] This may explain why it is the most widespread co-factor of enzymes involved in oxidative processes for instance. But the main reason may lie also in the reactivity of the FeO^{2+} moiety. The C−H hydroxylation by the FeO^{2+} moiety is generally described by an H-abstraction/O-rebound mechanism, as proposed about 30 years ago by Groves and co-workers.[27,28] The scheme of this mechanism is given Figure 1: in the first step, one hydrogen atom is abstracted from the alkyl species by the FeO^{2+} species, yielding an $FeOH^{2+}$ moiety together with a carbon radical (intermediate **I**); in the second step, this latter species collapses onto the hydroxyl oxygen. This rebound step is almost a barrierless process.[25] Consequently, the kinetics of the reaction is controlled by the first step **RC** → **I**, namely the H-abstraction step.

Table 1. Ligand Environment Influence on the FeO^{2+} Moiety As Illustrated on the $FeO(H_2O)_n(NH_3)_{5-n}^{2+}$, n = 5,4,1,0 Complexes by Bernasconi et al.[30] [a]

ligand		spin	lowest vacant acceptor orbital		
equatorial	axial	$(2S+1)$	label	energy (eV)	energy barrier (kJ/mol)
H_2O	H_2O	5	$3\sigma^*(\alpha)$	−13.6	23
H_2O	NH_3	5	$3\sigma^*(\alpha)$	−13.3	54
NH_3	H_2O	3	$2\pi_x^*(\beta)$	−11.9	111
NH_3	NH_3	3	$2\pi_x^*(\beta)$	−11.9	103

[a] Those data refer to BLYP calculations as detailed in this work.[30] Note the strong influence of the strength of the equatorial ligand field on the spin state, the nature and energy (in eV) of the lowest vacant orbital and as a consequence on the H-abstraction energy barrier (in kJ/mol). Note also the influence of the axial ligand in the high spin state on the $3\sigma^*$ energy: an increase in the ligand donation (from H_2O to NH_3) pushes up the $3\sigma^*$ and as a consequence, leads to a higher energy barrier (kJ/mol) for the H-abstraction step.

Let us then focus on the H-abstraction from an alkyl C−H bond by a FeO^{2+} species. The first issue is the presence and the role of different spin states of the oxidoiron species.[29] To investigate the FeO^{2+} reactivity as a function of the spin state, Bernasconi et al. have studied the electronic structure and the reactivity of $[FeO(H_2O)_n(NH_3)_{5-n}]^{2+}$, n = 5,4,1,0 (see Table 1).[30] From those results, one can notice that the triplet state is stabilized by a strong equatorial ligand field, such as created by NH_3, whereas the quintet state is stabilized by a weak equatorial ligand field such as created by H_2O. The reason is simple and lies in the orbital pattern depicted in Figure 2 in the H_2O versus NH_3 equatorial environment case. The ligands lying in the equatorial plane affect the energy of the orbitals lying in this plane, namely the $1\delta_{xy}$ and the $1\delta_{x^2-y^2}$. The stronger the ligand field is, the more destabilized those δ orbitals are. The destabilization shift depends on the orbital shape: the $1\delta_{x^2-y^2}$ orbital is more strongly destabilized than the $1\delta_{xy}$ orbital because of its lobes

(9) Reis, P.; Silva, J.; Palavra, A.; Da Silva, J.; Kitamura, T.; Fujiwara, Y.; Pombeiro, A. *Angew. Chem., Int. Ed.* **2003**, *42*, 821–823.
(10) Kirillova, M. V.; Kuznetsov, M. L.; Reis, P. M.; Da Silva, J. A. L.; Da Silva, J. J. R. F.; Pombeiro, A. J. L. *J. Am. Chem. Soc.* **2007**, *129*, 10531–10545.
(11) Kirillova, M. V.; Kuznetsov, M. L.; Da Silva, J. A. L.; Guedes Da Silva, M. F. C.; Da Silva, J. J. R. F.; Pombeiro, A. J. L. *Chem.−Eur. J.* **2008**, *14*, 1828–1842.
(12) Mardani, H. R.; Golchoubian, H. *J. Mol. Catal. A: Chem.* **2006**, *259*, 197–200.
(13) Groves, J. T. *J. Inorg. Biochem.* **2006**, *100*, 434–447.
(14) de Visser, S. P.; Shaik, S.; Sharma, P. K.; Kumar, D.; Thiel, W. *J. Am. Chem. Soc.* **2003**, *125*, 15779–15788.
(15) Shaik, S.; Kumar, D.; de Visser, S. P.; Altun, A.; Thiel, W. *Chem. Rev.* **2005**, *105*, 2279–2328.
(16) Altun, A.; Shaik, S.; Thiel, W. *J. Am. Chem. Soc.* **2007**, *129*, 8978–8987.
(17) Schöneboom, J. C.; Neese, F.; Thiel, W. *J. Am. Chem. Soc.* **2005**, *127*, 5840–5853.
(18) Bassan, A.; Blomberg, M. R. A.; Borowski, T.; Siegbahn, P. E. M. *J. Inorg. Biochem.* **2006**, *100*, 727–743.
(19) Krebs, C.; Fujimori, D. G.; Walsh, C. T.; Bollinger, J. M. *Acc. Chem. Res.* **2007**, *40*, 484–492.
(20) Yoshizawa, K.; Yumura, T.; Shiota, Y.; Yamabe, T. *Bull. Chem. Soc. Jpn.* **2000**, *73*, 29–36.
(21) Yang, G.; Zhou, D.; Liu, X.; Han, X.; Bao, X. *J. Mol. Struct.* **2006**, *797*, 131–139.
(22) Nam, W. *Acc. Chem. Res.* **2007**, *40*, 522–531.
(23) Buda, F.; Ensing, B.; Gribnau, M.; Baerends, E. J. *Chem.−Eur. J.* **2001**, *7*, 2775–2783.
(24) Ensing, B.; Buda, F.; Blöchl, P.; Baerends, E. J. *Angew. Chem., Int. Ed.* **2001**, *40*, 2893–2895.
(25) Ensing, B.; Buda, F.; Gribnau, M. C. M.; Baerends, E. J. *J. Am. Chem. Soc.* **2004**, *126*, 4355–4365.
(26) Earnshaw, A.; Greenwood, N. *Chemistry of the elements*; Butterworth-Heinemann: Woburn, MA, 1997.
(27) Groves, J. T.; McClusky, G. A. *J. Am. Chem. Soc.* **1976**, *98*, 859–861.
(28) Groves, J. T.; Vanderpuy, M. *J. Am. Chem. Soc.* **1976**, *98*, 5290–5297.
(29) Neese, F. *J. Inorg. Biochem.* **2006**, *100*, 716–726.
(30) Bernasconi, L.; Louwerse, M. J.; Baerends, E. J. *Eur. J. Inorg. Chem.* **2007**, 3023–3033.

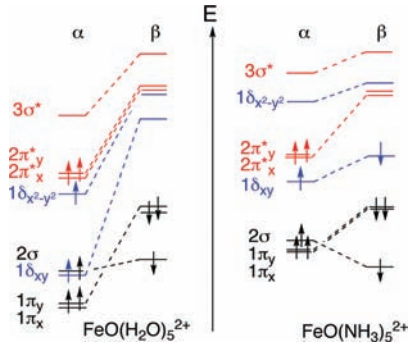

Figure 2. Simplified molecular orbital diagram for FeO^{2+} moiety in two different ligand environments: a weak equatorial ligand field environment (H_2O; left panel) favors the quintet spin state; a strong equatorial ligand field (NH_3; right panel) favors the triplet spin state. The most important orbitals are in color. The spin state is mainly controlled by the δ orbitals (in blue) whereas the reactivity is mainly controlled by the σ^* orbital (high spin configuration) or the π^* orbitals (low spin configuration) (in red).

pointing toward the ligands. When the destabilization is large enough, the $1\delta_{x^2-y^2}(\alpha)$ becomes then so high-lying that it loses its electron in favor of the $1\delta_{xy}(\beta)$, the complex switches from a high spin state (quintet) to a low spin state (triplet).

Thus, the spin state is essentially controlled by the strength of the equatorial field through the differential δ orbital destabilization. What about the reactivity? It has already been emphasized that the capability of the FeO^{2+} moiety to promote H-abstraction is directly connected to its electrophilicity: the C−H bond breaking is induced by electron donation from this C−H bond into a low lying empty molecular orbital of the FeO^{2+} species. This low lying empty orbital which accepts electronic density from the substrate is the *lowest acceptor molecular orbital*. It can be different from the lowest unoccupied molecular orbital (LUMO). Indeed, because of the hindrance of equatorial ligands, $1\delta_{x^2-y^2}$ and $1\delta_{xy}$ orbitals cannot accept density from the substrate C−H bond, but they can be the LUMO. The nature and the energy level of the lowest acceptor orbital depends on the spin state of this electrophilic species as illustrated by the $[FeO(H_2O)_n(NH_3)_{5-n}]^{2+}$, $n = 5, 4, 1, 0$ cases (see Table 1 and Figure 2). In a high spin configuration, the LUMO is the $1\delta_{xy}(\beta)$ orbital. The strong exchange field of the four unpaired α electrons stabilizes significantly the α orbitals. As a consequence, the $\sigma^*(\alpha)$ orbital is lying below the $2\pi^*(\beta)$ orbitals. It is the lowest acceptor orbital: it will accept electron donation from the C−H bond during the H-abstraction step. In the low spin configuration, the exchange field stabilization is weaker; hence, the $2\pi_x^*(\beta)$ orbital is both the LUMO and the lowest acceptor orbital. As seen previously, the strength of the equatorial ligand field controls the relative position of the 1δ energy levels—from which follow the spin state and the nature of the lowest acceptor orbital. It also controls the global position of the energy levels of the π and σ orbitals. Indeed, donating ligands such as NH_3 induce a global stronger destabilization of those orbitals and as a consequence they reduce the FeO^{2+} electrophilicity. To conclude, the choice of the equatorial ligands is crucial. A weak ligand field strongly enhances the electrophilicty of the FeO^{2+} moiety: (1) orbitals are relatively low lying in energy, (2) the high spin state stabilizes the lowest lying vacant orbital ($3\sigma^*(\alpha)$) by the strong exchange field.

Last but not least, what about the influence of the axial ligand field? The axial ligand may affect the molecular orbitals lying along the z axis, namely the σ and π orbital. Indeed, according to Bernasconi et al.,[30] a stronger σ-donating ligand pushes up the $3\sigma^*$. Thus, the electrophilicity of the FeO^2 is reduced, the H-abstraction energy barrier is higher. For instance, replacing H_2O by NH_3 in axial position of the $FeO(H_2O)_5^{2+}$ complex leads to a higher lying $3\sigma^*(\alpha)$ (from −13.6 eV to −13.3 eV) and a higher energy barrier (from 23 to 54 kJ/mol) (see Table 1). This effect can be used to tune the reactivity of a FeO^{2+} complex in high spin configuration.[30,31]

In summary: (1) a wide range of transition metals can be used to perform oxidation reactions; (2) the FeO^{2+} moiety is a widespread active species in alkyl hydroxylation, from zeolites to enzymes; (3) the strong reactivity of the high spin FeO^{2+} moiety results from its electronic structure: the low lying $3\sigma^*(\alpha)$ vacant orbital is responsible for its strong electrophilicity, making it accept electrons even from poor donating entities such as aliphatic C−H bonds. We thus understand the role of the ligand environment on the reactivity of the FeO^{2+} species. In this article, we will focus on the role of the metal. We present here an extensive study in gas phase of the methane-to-methanol reaction catalyzed by the first row transition-metal oxide-dications $MO(H_2O)_p^{2+}$ (M = V, Cr, Mn, Fe, Co, $p = 5$ and M = Ni, Cu, $p = 4$). The electronic structure analysis together with the reactive scheme for each complex allow us to discuss the relative importance of the vacant $3\sigma^*$ compared with the vacant $2\pi^*$ and to highlight the great importance of the "d count" on the reactivity of those complexes.

Method

Level of Theory. All the calculations have been performed using the ADF (Amsterdam Density Functional) package,[32−35] using the OPBE density functional.[36,37] This functional has been chosen for its performance in describing close-lying spin states, in particular in iron complexes.[38] In the ADF code, the electronic orbitals are written in terms of Slater-type orbitals (STO). We use a triple-ζ basis set with two polarization functions for the C, O, and H atoms and a quadruple zeta basis set with three polarization functions for the transition metal atoms, as available in the ADF library of standard basis sets. Additionally, the calculations were corrected for relativistic effects using the zero-order regular approximation (ZORA) approach.[39,40] When needed, the frequencies are computed

(31) Bernasconi, L.; Baerends, E. J. *Eur. J. Inorg. Chem.* **2008**, 1672–1681.
(32) Bickelhaupt, F.; Baerends, E. *Rev. Comp. Chem.* **2000**, *15*, 1–86.
(33) Baerends, E. J.; Ellis, D. E.; Ros, P. *Chem. Phys.* **1973**, *2*, 41–51.
(34) Velde, G. T.; Bickelhaupt, F. M.; Baerends, E. J.; Guerra, C. F.; Van Gisbergen, S. J. A.; Snijders, J. G.; Ziegler, T. *J. Comput. Chem.* **2001**, *22*, 931–967.
(35) *SCM, ADF2006.01*; Theoretical Chemistry,Vrije Universiteit Amsterdam: The Netherlands, 2006; http://www.scm.com/.
(36) Perdew, J. P.; Burke, K.; Ernzerhof, M. *Phys. Rev. Lett.* **1997**, *78*, 1396.
(37) Cohen, A. J.; Handy, N. C. *Mol. Phys.* **2001**, *99*, 607–615.
(38) Swart, M.; Ehlers, A.; Lammertsma, K. *Mol. Phys.* **2004**, *102*, 2467–2474.
(39) van Lenthe, E.; Baerends, E. J.; Snijders, J. G. *J. Chem. Phys.* **1994**, *101*, 9783–9792.
(40) van Lenthe, E.; Ehlers, A.; Baerends, E. J. *J. Chem. Phys.* **1999**, *110*, 8943–8953.

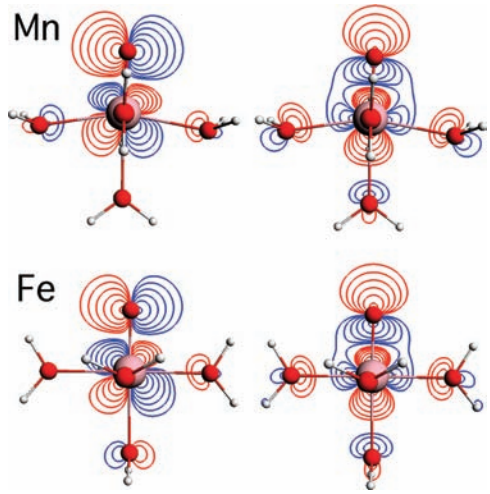

Figure 3. $2\pi_x^*(\alpha)$ (left side) and $3\sigma(\alpha)^*$ (right side) molecular orbitals of the $MnO(H_2O)_5^{2+}$ (top) and $FeO(H_2O)_5^{2+}$ (bottom) in the ground state.

analytically. All the transition state structures have been characterized by the presence of an imaginary frequency.

Chosen Systems. To better understand the reactivity of the MO^{2+} moiety toward aliphatic C−H bonds, it is crucial to take into account its ligand environment. Indeed, as seen in the Introduction, it influences the electronic structure and the spin state of the MO^{2+} moiety, hence its reactivity toward a C−H bond. To study the influence of the metal, we have chosen to study a hydrated MO^{2+} moiety.

First, the presence of ligands prevents methane from interacting directly with the transition metal. For the bare oxo MO^+ in gas phase, Shiota and Yoshizawa propose for instance a reactant complex OM-CH_4^+ where the methane interacts directly with the metal and an intermediate HOM-CH_3^+, which exhibits a metal−carbon bond.[41] Such a mechanism is strongly disadvantaged if the metal is surrounded by ligands.[25]

In our study of the influence of the "d count" on the reactivity of the MO^{2+} moiety, we have chosen to focus on the first row transition metal series, from vanadium to copper. The chosen systems are then the $MO(H_2O)_p^{2+}$ complexes (M = V, Cr, Mn, Fe, Co, Ni, Cu). They can be divided into two groups according to the number p of water molecules in the first solvation shell of the MO^{2+} moiety.

• $p = 5$: for M = V, Cr, Mn, Fe, Co, the $MO(H_2O)_5^{2+}$ complex is pseudo-octahedral, keeping almost the same geometry along the series. The M=O distance is slightly increasing from 1.54 Å to 1.59 Å when going from V to Co. The metal-water distances are between 2.05 Å and 2.15 Å in general (see the iron case in Figure 4 and Table 2).

• $p = 4$: for M = Ni, Cu, the $MO(H_2O)_4^{2+}$ complex presents a strongly distorted trigonal bipyramid geometry coordination, the oxo group lying in the trigonal plane (see Figure 5 and Table 2). Some species along the reaction path can afford an extra water molecule such as $NiO(H_2O)_4^{2+}$ in high spin state ($2S + 1 = 5$). However, most of the species along the reaction path cannot afford an extra water molecule in their coordination sphere: all attempts to optimize the geometry of $NiO(H_2O)_4^{2+}$ in low spin state or $CuO(H_2O)_4^{2+}$ in both spin states result in the dissociation of one metal-water bond. We therefore keep in all cases the coordination shell constant at four water molecules along the entire reaction path.

(41) Shiota, Y.; Yoshizawa, K. *J. Am. Chem. Soc.* **2000**, *122*, 12317–12326.

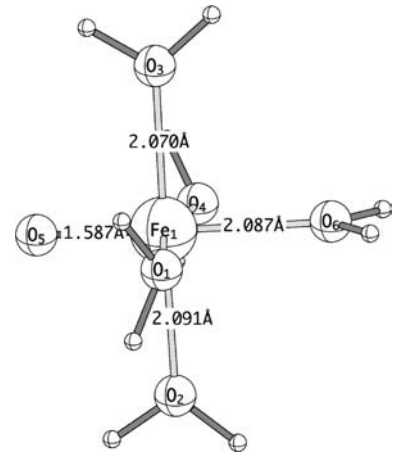

Figure 4. Structure of $FeO(H_2O)_5^{2+}$, high spin state. Distances are given in angstrom. See Table 2 for data on angles.

Table 2. Geometrical Data for $MO(H_2O)_p^{2+}$, M = Fe and $p = 5$, M = Ni, Cu and $p = 4$ in Their Ground State[a]

angle	Fe	Ni	Cu
O1−M−O2	87.8	93.0	107.7
O1−M−O3	92.7	87.8	94.6
O1−M−O4	168.5	129.4	91.1
O1−M−O5	95.0	110.3	108.0
O1−M−O6	85.0		
O2−M−O3	178.9	165.8	157.1
O2−M−O4	87.2	85.9	87.2
O2−M−O5	90.6	97.4	88.3
O2−M−O6	90.3		
O3−M−O4	91.9	82.6	87.6
O3−M−O5	90.3	95.6	89.2
O3−M−O6	88.8		
O4−M−O5	95.5	119.9	160.7
O4−M−O6	84.5		
O4−M−O5	179.1		

[a] Angles are in degree. See Figure 4 and Figure 5 for notations.

Results and Discussion

First, we will focus on the electronic structure of the MO^{2+} moiety in the $MO(H_2O)_p^{2+}$ complexes. Then, we will expose the reaction scheme of the methane hydroxylation catalyzed by those complexes. Those results will provide us some clues to answer the questions raised in the introduction: what is the relative importance of the vacant $3\sigma^*$ compared with the vacant $2\pi^*$ orbital? what is the importance of the "d count" on the reactivity of the MO^{2+} species? what singles out FeO^{2+}?

Electronic Structure of the MO^{2+} Moiety. The electronic structure of the $MO(H_2O)_p^{2+}$ complex is reported in Table 3. All along the series, the M−O bonding results from the filling of the 1π and 2σ orbitals, which are $M_{3d}-O_{2p}$ bonding orbitals. From V to Fe, each added electron occupies an extra α orbital, stabilized by the exchange field: $1\delta_{x^2-y^2}(\alpha)$ in the chromium complex, $2\pi_x^*(\alpha)$ in the manganese complex, $2\pi_y^*(\alpha)$ in the iron complex. As a consequence, the spin state increases regularly from doublet to quintet. Then, the next step is cobalt. Whereas the spin state of the bare oxo complex CoO^{2+} is a sextet, the extra electron occupies a β orbital ($1\delta_{xy}(\beta)$) in the $CoO(H_2O)_5^{2+}$ complex, leading to a quartet

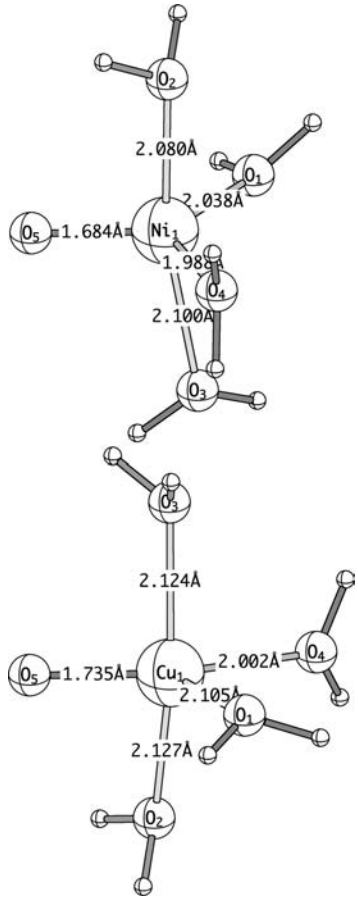

Figure 5. Structures of $MO(H_2O)_4^{2+}$, M = Ni, Cu, high spin state. Distances are given in angstrom. See Table 2 for data on angles.

Table 3. Spin State ($2S + 1$) and Electronic Configuration of the Ground State of $MO(H_2O)_p^{2+}$ (for M = V, Cr, Mn, Fe, Co, $p = 5$; for M = Ni, Cu, $p = 4$)

metal	spin ($2S + 1$)	configuration
V	2	$(2\sigma)^2\,(1\pi_x)^2\,(1\pi_y)^2\,1\delta_{xy}$
Cr	3	$(2\sigma)^2\,(1\pi_x)^2\,(1\pi_y)^2\,1\delta_{xy}\,1\delta_{x^2-y^2}$
Mn	4	$(2\sigma)^2\,(1\pi_x)^2\,(1\pi_y)^2\,1\delta_{xy}\,1\delta_{x^2-y^2}\,2\pi_x^*$
Fe	5	$(2\sigma)^2\,(1\pi_x)^2\,(1\pi_y)^2\,1\delta_{xy}\,1\delta_{x^2-y^2}\,2\pi_x^*\,2\pi_y^*$
Co	4	$(2\sigma)^2\,(1\pi_x)^2\,(1\pi_y)^2\,(1\delta_{xy})^2\,1\delta_{x^2-y^2}\,2\pi_x^*\,2\pi_y^*$
Ni	5	$(2\sigma)^2\,(1\pi_x)^2\,(1\pi_y)^2\,(1\delta_{xy})^2\,1\delta_{x^2-y^2}\,2\pi_x^*\,2\pi_y^*\,3\sigma^*$
Cu	4	$(2\sigma)^2\,(1\pi_x)^2\,(1\pi_y)^2\,(1\delta_{xy})^2\,(1\delta_{x^2-y^2})^2\,2\pi_x^*\,2\pi_y^*\,3\sigma^*$

spin state for the ground state. Then, in nickel and copper, the extra electron occupies successively the $3\sigma^*(\alpha)$ and the $1\delta_{x^2-y^2}(\beta)$, leading to two complexes with all 3d α orbitals filled.

We have already emphasized in the Introduction the importance of the *lowest lying acceptor orbital* for the electrophilic properties of the FeO^{2+} moiety. Along this series, it can be either a σ^* orbital or a π^* orbital. These orbitals are illustrated with plots of the $3\sigma^*(\alpha)$ and the $2\pi^*(\alpha)$ for Mn and Fe complexes in Figure 3.

Table 4 gives some properties of the lowest vacant $3\sigma^*$, the lowest vacant $2\pi^*$, and the LUMO (which may or may not be the $2\pi^*$ or $3\sigma^*$): energy, spin, composition in terms of d metal and p oxygen percentage ($\%d_M$ and $\%p_O$). In Figure 6, we plot the most important molecular orbital energies as a function of the metal: $2\pi^*(\alpha)$, $3\sigma^*(\alpha)$, $1\delta_{xy}(\beta)$, $1\delta_{x^2-y^2}(\beta)$, $2\pi^*(\beta)$, and $3\sigma^*(\beta)$ (in order of increasing energy). From this table and Figure 6, the first striking fact is that the molecular orbital energy decreases when the atomic number of M increases: it is due to the higher nuclear charge along the series. A closer analysis of those results leads us to divide the studied complexes into three groups according to the lowest vacant orbital:

Table 4. Selected Vacant Molecular Orbitals (Energy in eV) for the Ground State of $MO(H_2O)_p^{2+}$ (for M = V, Cr, Mn, Fe, Co, $p = 5$; for M = Ni, Cu, $p = 4$)[a]

	LUMO					lowest vacant $3\sigma^*$					lowest vacant $2\pi^*$				
metal	label		E	spin	$\%d_M$	$\%p_O$	E	spin	$\%d_M$	$\%p_O$	E	spin	$\%d_M$	$\%p_O$	E
V	$2\pi^*(\alpha)$		−12.2	α	45	20	−10.1	α	64	29	−12.2				
Cr	$2\pi^*(\alpha)$		−13.8	α	44	25	−12.0	α	44	32	−13.8				
Mn	$2\pi^*(\alpha)$		−14.8	α	43	32	−13.2	α	34	59	−14.8				
Fe	$\delta_{xy}(\beta)$		−14.3	α	40	36	−13.9	β	50	35	−13.2				
Co	$3\sigma^*(\alpha)$		−14.5	α	42	30	−14.5	β	47	47	−14.1				
Ni	$1\delta_{x^2-y^2}(\beta)$		−15.7	β	26	18	−14.8	β	63	18	−15.4				
Cu	$2\pi^*(\beta)$		−16.3	β	36	18	−15.8	β	16	58	−16.3				

[a] The molecular orbital spin is provided together with its composition in terms of d metal orbitals percentage ($\%d_M$) and p oxygen orbitals ($\%p_O$) percentage.

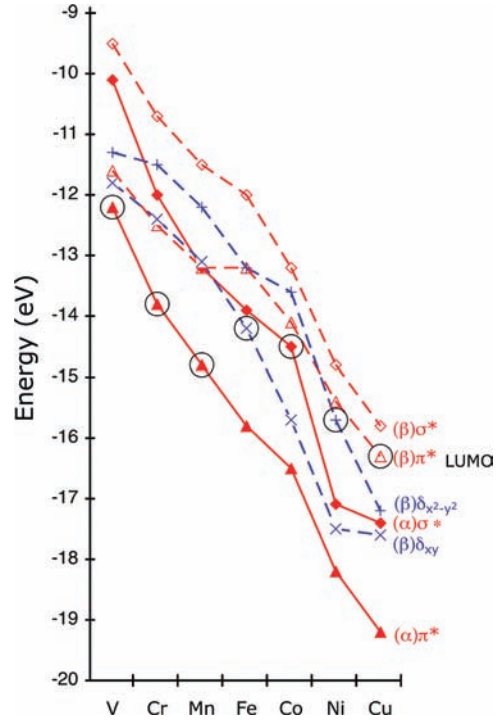

Figure 6. Energies of molecular orbitals of interest (in eV) for the studied complexes ($MO(H_2O)_p^{2+}$, M = V, Cr, Mn, Fe, Co, $p = 5$; for M = Ni, Cu, $p = 4$). As a guide to the eye, we connect the same orbitals with a line that is solid for α orbitals and dashed for β orbitals. For the sake of simplicity, π_x and π_y are not distinguished. The LUMO orbital is highlighted by a black circle.

M = V, Ce, Mn. In this group, the lowest acceptor orbital is a $2\pi^*(\alpha)$ orbital. It is also the LUMO.

M = Fe, Co. In this group, the lowest acceptor orbital is the $3\sigma^*(\alpha)$ orbital. In the iron case, it differs from the LUMO ($1\delta_{xy}(\beta)$), for Co, it is the LUMO.

M = Cu, Ni. In this group, the lowest acceptor orbital is a $2\pi^*(\beta)^*$ orbital. In the nickel case, it differs from the LUMO ($1\delta_{x^2-y^2}(\beta)$), for Cu, it is the LUMO.

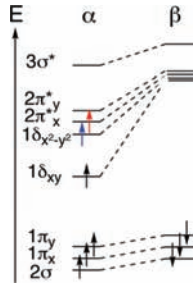

Figure 7. Simplified molecular orbital diagram of $MO(H_2O)_5^{2+}$, M = V, Cr, Mn. The black spins represent the occupation in the vanadium case. For the chromium complex, the supplementary spin (here in blue) occupies the $1\delta_{x^2-y^2}(\alpha)$ orbital. Then, for the manganese complex, the second extra electron (here in red) occupies the $2\pi_x^*(\alpha)$ orbital. For the sake of simplicity, we have not shown here the crossing between $2\pi_x^*(\alpha)$ and the $\delta_{x^2-y^2}$ when switching from the vanadium to the chromium complex. The main consequence of the energy levels crossing is that the LUMO in both complexes is the $2\pi_x^*(\alpha)$ molecular orbital.

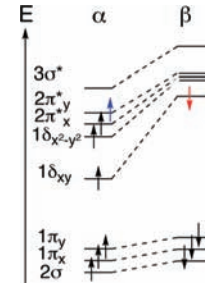

Figure 8. Simplified molecular orbital diagram of $MO(H_2O)_5^{2+}$, M = Fe, Co. The black spins represent the occupation in the manganese case. For the iron complex, the supplementary spin (here in blue) occupies the $2\pi_y^*(\alpha)$ orbital. Then, for the cobalt complex, the second extra electron (here in red) occupies the $1\delta_{xy}(\beta)$ orbital.

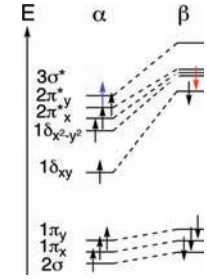

Figure 9. Simplified molecular orbital diagram of $MO(H_2O)_4^{2+}$, M = Ni, Cu. The black spins represent the occupation in the cobalt case. For the nickel complex, the supplementary spin (here in blue) occupies the $3\sigma^*(\alpha)$ orbital. Then, for the copper complex, the second extra electron (here in red) occupies the $1\delta_{x^2-y^2}(\beta)$ orbital.

Let us consider the electronic structure within each group.

V, Cr, Mn. A schematic orbital energy diagram of this group is given Figure 7. From V to Mn, each added electron occupies an extra α orbital, stabilized by the exchange field: $1\delta_{x^2-y^2}(\alpha)$ in Cr complex, $2\pi_x^*(\alpha)$ in Mn complex. The spin state increases from doublet to quartet.

Along this group, very few crossings of energy levels occur. The most noticeable one is the crossing of the $2\pi_x^*(\alpha)$ level from below the $1\delta_{x^2-y^2}(\alpha)$ level in the vanadium complex to above the $1\delta_{x^2-y^2}(\alpha)$ level in the chromium complex. For the sake of simplicity, we only represent the orbital ordering for the Cr and Mn cases in the simplified orbital energy diagram of Figure 7. The consequence of this swap is that even with one more α electron in the chromium complex, the lowest acceptor orbital is the same ($2\pi_x^*(\alpha)$) in both the V and Cr complexes.

Thus, in this group, the lowest vacant acceptor orbital, which is also the LUMO, is a $2\pi^*(\alpha)$ orbital, namely the $2\pi_x^*(\alpha)$ orbital for V and Cr and the $2\pi_y^*(\alpha)$ for Mn. Two factors have to be taken into account to predict the electrophilicity of the MO^{2+} moiety: the energy of the lowest vacant orbital, $\varepsilon_{2\pi^*(\alpha)}$, and its oxygen p orbital contribution, $\%p_O$. Generally speaking, the lower the acceptor orbital lies in energy and the higher the $\%p_O$ is, the more electrophilic the MO^{2+} will be: they are both in favor of a large electronic donation from the C−H bond into the MO^{2+} acceptor orbital. Within the series (V, Cr, Mn), $\varepsilon_{2\pi^*(\alpha)}$ is strongly decreasing (from −12.2 eV to −14.8 eV) while $\%p_O$ is strongly increasing (from 29% to 59%), see Figure 6 and Table 4. So, from V to Mn, the $MO(H_2O)_5^{2+}$ complex should be more and more efficient in performing H-abstraction from methane.

Previous studies have demonstrated the high reactivity of the $FeO(H_2O)_5^{2+}$ complex. The lowest acceptor orbital of this complex is the $3\sigma^*(\alpha)$, lying at −13.9 eV. Thus, on the basis of the energy level of the lowest acceptor orbital, one should expect the Mn complex to be even more efficient than the Fe complex. However, the nature of the lowest acceptor orbital differs ($2\pi^*(\alpha)$ versus $3\sigma^*(\alpha)$). In the $2\pi^*$ case, the overlap efficiency requires sideways approach, leading to steric hindrance of the incoming organic substrate molecule (e.g., CH_4) with the equatorial water ligands. This competition may reduce the Mn complex oxidative activity.

Fe, Co. A schematic orbital energy diagram is given in Figure 8. From Mn to Fe, the extra electron goes into the $2\pi_y^*(\alpha)$, leading to the expected high spin configuration (quintet) for the $FeO(H_2O)_5^{2+}$ complex. In the $CoO(H_2O)_5^{2+}$ complex case, the extra electron occupies a β orbital, leading to a quartet spin state for the ground state.[42] Thus, for both iron and cobalt, the $2\pi^*(\alpha)$ is doubly occupied and the lowest acceptor orbital is the $3\sigma^*(\alpha)$ orbital. We have already pointed out that the two main parameters which can control the electrophilicity of the complex are the energy and the $2p_O$ contribution of the lowest lying vacant orbital. The $3\sigma^*(\alpha)$ energy and the $2p_O$ contribution are similar in both complexes: the cobalt complex $3\sigma^*(\alpha)$ lies 0.6 eV below the iron complex $3\sigma^*(\alpha)$ (see Figure 6), but its p_O contribution is slightly less favorable (30% vs 36%), see Table 4. Previous studies have demonstrated the high reactivity of $FeO(H_2O)_5^{2+}$ complex. Even if cobalt has been used much less than iron in oxidative processes, it is clear that cobalt complexes should be as reactive as iron complexes, if not more so.

Ni, Cu. A schematic molecular diagram is given in Figure 9. We have already set apart those two complexes because of a reduced number of water ligands in the coordination shell. They can also be distinguished through their electronic structure. All the α orbitals of interest are occupied: from

(42) Cobalt is the only case where the spin state of the complex $MO(H_2O)_p^{2+}$ differs from the spin state of the bare oxo MO^{2+}.

Table 5. Studied Reaction: $MO(H_2O)_p^{2+} + CH_4 \rightarrow M(H_2O)_p^{2+} + CH_3OH$, i.e., **R** → **P**[a]

	spin ($2S + 1$)		
metal	**R**	**P**	ΔE (kJ/mol)
V	2	4	149.1
Cr	3	5	−46.0
Mn	4	6	−206.8
Fe	5	5	−119.1
Co	4	4	−153.8
Ni	5	3	−218.8
Cu	4	2	−302.4

[a] For each metal, this table gives the spin state of the reactant **R** and product **P** ground state and ΔE, the energetic cost of the reaction (in kJ/mol).

cobalt to nickel complex, the extra electron occupies the $3\sigma^*(\alpha)$ leading to a quintet spin state. Then, from nickel to copper, the extra electron is added into the $1\delta_{x^2-y^2}$ orbital. Thus, in both complexes, the lowest lying acceptor orbital is a $2\pi^*(\beta)$. As seen previously, the energy and the composition of this $2\pi^*(\beta)$ orbital determine the electrophilicity of the complex. In the copper complex, the $2\pi^*(\beta)$ lies at a lower energy (−16. eV vs −15.4 eV) and its $2p_O$ contribution is larger (58% vs 18%) than in the nickel complex. So, we can assume that this complex may be more reactive than the Ni complex to perform alkyl hydroxylation.

Anyway, both Ni and Cu complexes seem very promising to promote C−H oxidation based on the lowest vacant orbital energy level (at least 1 eV lower than the iron one). The nature of the lowest acceptor orbital ($2\pi^*(\beta)$) may reduce the efficiency of those complexes because of the overlap/steric hindrance of the water ligands upon the sideways approach of a substrate molecule, which is required for optimal overlap with $2\pi^*$ orbitals. The lower number of water molecules should however reduce the impact of this competition. However, very little is known about the stability of those complexes as active intermediates in oxidative catalysis.

Along the Series. The energy of the lowest acceptor orbital and its $2p_O$ orbital contribution are a bit less favorable in Fe and Co complex than in the Mn or Cu complex. However, for iron and cobalt, the lowest acceptor orbital is the $3\sigma^*(\alpha)$, not a $2\pi^*$ orbital. As noted, the overlap between the acceptor orbital and the C−H bonding orbital may be lower with a $2\pi^*$ orbital than with a $3\sigma^*$ orbital because of the steric hindrance of the ligands. Thus, no conclusion can be drawn yet concerning the H-abstraction capability of all these complexes. To investigate further the $MO(H_2O)_p^{2+}$ reactivity toward the C−H bond, we have made an extensive study of the intermediates and transition states involved in the $CH_4 + MO(H_2O)_p^{2+} \rightarrow M(H_2O)_p^{2+} + CH_3OH$ reaction.

Mechanism. Overview. In Table 5, data concerning the **R** → **P** reaction are collected: energetic cost $\Delta E = E(P) - E(R)$, spin state of the reactants **R**, spin state of the products **P**. Except in the vanadium case, this reaction is exoenergetic. The energetic cost decreases from V (149.1 kJ/mol) to Cu (−302.4 kJ/mol) and is particularly low in the Mn case (−206.8 kJ/mol). Moreover, this reaction implies a spin crossing, except for iron and cobalt.

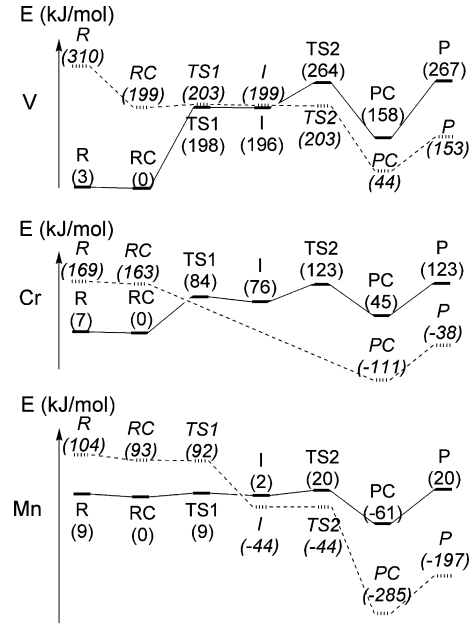

Figure 10. Energy profile (in kJ/mol) for the methane to methanol conversion catalyzed by $MO(H_2O)_5^{2+}$, M = V, Cr, Mn. Dashed line stands for the high spin mechanism and continuous line for the low spin mechanism. Along the reaction coordinate, the following species have been characterized: the reactants $MO(H_2O)_5^{2+}$ and CH_4 (**R**); the reactant complex [$MO(H_2O)_5^{2+}$, CH_4] (**RC**); the transition state corresponding to the H-abstraction step (**TS1**); the intermediate [$MOH(H_2O)_5^{2+}\cdots{}^{\cdot}CH_3$], (**I**); the transition state corresponding to the rebound step (**TS2**); the product complex $MCH_3OH(H_2O)_5^{2+}$ (**PC**); the products $M(H_2O)_5^{2+}$ and CH_3OH (**P**).

This reaction follows a rebound mechanism (see Figure 1).[25] First, one hydrogen atom is abstracted from the substrate, here CH_4. This yields intermediate **I** ($MOH(H_2O)_p^{2+} + {}^{\cdot}CH_3$. Then, the carbon radical ${}^{\cdot}CH_3$ can collapse onto the hydroxo group to yield the product complex **PC** ($M(OHCH_3)(H_2O)_p^{2+}$). The energy profile of those steps is given in Figure 10 for the V, Cr and Mn complexes, in Figure 11 for the Fe and Co complexes, and in Figure 12 for the Ni and Cu complexes.

The rebound step is relatively uninteresting, being very smooth. Data concerning this step are collected in Table 6: spin evolution, energetic cost $\Delta E_2 = E(P) - E(I)$, energy barrier $\Delta E_{TS2}^{\ddagger}$, C−O distance and MOC angle in the transition state structure. This step is highly exoenergetic in all cases. It is a non-activated process or with very low activation barrier $\Delta E_{TS2}^{\ddagger}$. Thus, we will mainly focus on the H-abstraction step, which controls the reaction kinetics. We will put in evidence the strong link between the activation energy $\Delta E_{TS1}^{\ddagger}$, and the transition state structure (**TS1**) on one hand and the lowest lying acceptor orbital of the $MO(H_2O)_p^{2+}$ complex on the other hand. In the previous section, we have discussed the electronic structure of the $MO(H_2O)_p^{2+}$ complexes. To supplement this, we have also performed a detailed study of the electronic structure of the H-abstraction transition state structures (**TS1**) thanks to a fragment interaction analysis. We have chosen to focus on the interaction between two fragments[43] in the transition state geometry: (i) the fragment $MO(H_2O)_p^{2+}$ (ii) the fragment CH_4. The

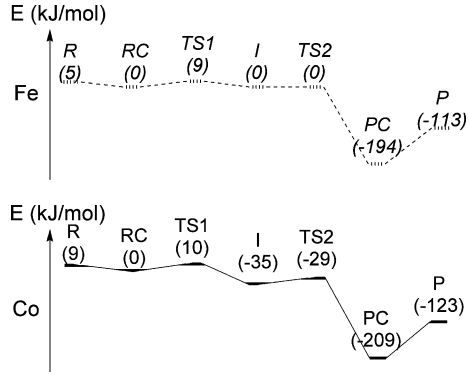

Figure 11. Energy profile (in kJ/mol) for the methane to methanol conversion catalyzed by $MO(H_2O)_5^{2+}$, M = Fe, Co. Dashed line stands for the high spin mechanism and continuous line for the low spin mechanism. Along the reaction coordinate, the following species have been characterized: the reactants $MO(H_2O)_5^{2+}$ and CH_4 (**R**); the reactant complex [$MO(H_2O)_5^{2+}$, CH_4] (**RC**); the transition state corresponding to the H-abstraction step (**TS1**); the intermediate [$MOH(H_2O)_5^{2+}\cdots CH_3$] (**I**); the transition state corresponding to the rebound step (**TS2**); the product complex $MCH_3OH(H_2O)_5^{2+}$ (**PC**); the products $M(H_2O)_5^{2+}$ and CH_3OH (**P**).

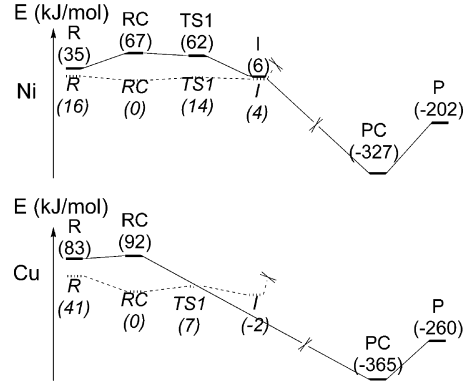

Figure 12. Energy profile (in kJ/mol) for the methane to methanol conversion catalyzed by $MO(H_2O)_4^{2+}$, M = Ni, Cu. Dashed line stands for the high spin mechanism and continuous line for the low spin mechanism. Along the reaction coordinate, the following species have been characterized: the reactants $MO(H_2O)_4^{2+}$ and CH_4 (**R**); the reactant complex [$MO(H_2O)_4^{2+}$, CH_4] (**RC**); the transition state corresponding to the H-abstraction step (**TS1**); the intermediate [$MOH(H_2O)_5^{2+}\cdots CH_3$] (**I**); the transition state corresponding to the rebound step (**TS2**); the product complex $MCH_3OH(H_2O)_4^{2+}$ (**PC**); the products $M(H_2O)_4^{2+}$ and CH_3OH (**P**).

Table 6. Data for the Rebound Step: **I** → **PC**[a]

	spin state					
metal	**I**	**PC**	ΔE_2 (kJ/mol)	$\Delta E^{\ddagger}_{TS2}$ (kJ/mol)	C−O (Å)	MOC (deg)
V	2	4	−37.3	7.5	2.12	140
Cr	3	6	−187.5			
Mn	6	6	−249.5	0	3.33	173
Fe	5	5	−194.9	0	2.59	135
Co	4	4	−173.1	6.6	3.00	159
Ni	3	3	−331.1			
Cu	2	2	−363.2			

[a] For each metal, this table gives the spin state ($2S+1$) of **I** and **PC** ground state and the energetic cost of the reaction $\Delta E_2 = E(PC) - E(I)$ (in kJ/mol). It provides also the activation energy $\Delta E^{\ddagger}_{TS2}$ (kJ/mol), the CO distance (in Å), and the MOC angle (in degree) in the transition state structure **TS2**.

gross population of the interesting fragment molecular orbitals in the transition state structure **TS1** are given in Table 8. The overlaps between the σ_{C-H} orbital of the stretched C−H bond and the $2\pi^*$ and $3\sigma^*$ orbitals of the complexes are given in Table 9.

Table 7. Studied Reaction: **RC** → **I**[a]

	spin state							lowest vacant acceptor MO	
metal	**RC**	**I**	ΔE_1 (kJ/mol)	$\Delta E^{\ddagger}_{TS1}$ (kJ/mol)	C−H (Å)	O−H (Å)	MOH (deg)	label	energy (eV)
V	2	2	196.3	198.9	1.76	1.04	128	$2\pi^*(\alpha)$	−12.2
Cr	3	3	76.3	84.9	1.39	1.17	125	$2\pi^*(\alpha)$	−13.8
Mn	4	6	−44.7	9.7	1.34	1.20	126	$2\pi^*(\alpha)$	−14.8
Fe	5	5	0.7	9.2	1.25	1.32	179	$3\sigma^*(\alpha)$	−13.9
Co	4	4	−35.0	11.7	1.34	1.19	177	$3\sigma^*(\alpha)$	−14.5
Ni	5	5	4.1	14.5	1.38	1.20	123	$2\pi^*(\beta)$	−15.4
Cu	4	4	−2.5	6.8	1.30	1.28	125	$2\pi^*(\beta)$	−16.3

[a] For each metal, this table gives the spin state ($2S+1$) of **RC** and **I** (ground states) and the energetic cost ΔE_1 of the reaction (in kJ/mol). It provides also the activation energy $\Delta E^{\ddagger}_{TS1}$, the OH distance (in Å) and the MOH angle (in degree) in the transition state structure **TS1**. The last two columns are a reminder of the key data concerning the lowest vacant acceptor molecular orbital: label and energy (in eV).

Table 8. Fragment Analysis of the Transition State Structure **TS1** for Each Complex $MO(H_2O)_p^{2+}$ (M = V, Cr, Mn, Fe, Co, $p = 5$; for M = Ni, Cu, $p = 4$)[a]

	α				β			
metal	$2\pi^*_x$	$2\pi^*_y$	$3\sigma^*$	σ_{C-H}	$2\pi^*_x$	$2\pi^*_y$	$3\sigma^*$	σ_{C-H}
V	0.43	0.40	0.02	0.28	0.05	0.05	0.02	0.89
	+0.43	*+0.40*	*+0.02*	*−0.72*	*+0.05*	*+0.05*	*+0.02*	*−0.11*
Cr	0.99	0.67	0.02	0.46	0.03	0.06	0.02	0.91
	+0.99	*+0.67*	*+0.02*	*−0.54*	*+0.03*	*+0.06*	*+0.02*	*−0.09*
Mn	0.74	0.96	0.04	0.43	0.09	0.03	0.03	0.91
	+0.74	*−0.04*	*+0.04*	*−0.57*	*+0.09*	*+0.03*	*+0.03*	*−0.09*
Fe	0.97	0.97	0.51	0.63	0.01	0.01	0.14	0.87
	−0.03	*−0.03*	*+0.51*	*−0.37*	*+0.01*	*+0.01*	*+0.14*	*−0.13*
Co	0.99	0.99	0.67	0.43	0.04	0.04	0.10	0.88
	−0.01	*−0.01*	*+0.67*	*−0.57*	*+0.04*	*+0.04*	*+0.10*	*−0.12*
Ni	0.97	0.97	0.98	0.94	0.29	0.34	0.09	0.37
	−0.03	*−0.03*	*−0.02*	*−0.06*	*+0.29*	*+0.34*	*+0.09*	*−0.63*
Cu	0.97	0.98	0.99	0.96	0.48	0.16	0.07	0.41
	−0.03	*−0.02*	*−0.01*	*−0.04*	*+0.48*	*+0.16*	*+0.07*	*−0.59*

[a] The two fragments are $MO(H_2O)_p^{2+}$ and CH_4. In this table, the gross populations of the relevant fragment molecular orbitals are given: the $2\pi^*$ and $3\sigma^*$ of the complex and the σ_{C-H} of the methane. In italic, the difference between the integer gross population in the isolated fragment and the gross population in the transition state. The orbitals have been defined in spin restricted calculations on the isolated fragments in the geometry they have in **TS1**.

Data related to the H-abstraction step are collected in Table 7: spin state evolution, energetic cost (ΔE_1), and activation energy barriers ($\Delta E^{\ddagger}_{TS1}$), selected geometrical data of the transition state structures (**TS1**). We have also added some key features of the electronic structure of the reactant $MO(H_2O)_p^{2+}$.

As we already noticed, this series can be divided into three groups according to the lowest acceptor orbital of the $MO(H_2O)_p^{2+}$ complex. We keep this subdivision to discuss the mechanism of the reaction $CH_4 + MO(H_2O)_p^{2+} \rightarrow M(H_2O)_p^{2+} + CH_3OH$. Before entering the discussion of the three groups we note that the calculated transition barriers are for gas phase reactions, and therefore much lower than

(43) The orbitals of the fragments are obtained in spin restricted calculations on the fragments with the geometries they have in the transition state. The orbital occupations have been enforced to yield electronic structures for the fragments that conform to the situation in the complex.

Table 9. Overlaps between the Highest σ Molecular Orbital of the CH_4 Fragment and the Molecular Orbitals of Interest of the Metal Complex Are Given for the Transition State Structure **TS1** of Each Complex $MO(H_2O)_p^{2+}$ (M = V, Cr, Mn, Fe, Co, $p = 5$; for M = Ni, Cu, $p = 4$)[a]

metal	$2\pi_x^*$	$2\pi_y^*$	$3\sigma^*$
V	0.0783	0.093	0.0583
Cr	0.0035	0.1147	0.05605
Mn	0.1171	0.0334	0.05317
Fe	0.0031	0.0021	0.1200
Co	0.0088	0.0063	0.1378
Ni	0.1029	0.1207	0.0891
Cu	0.1359	0.0813	0.0770

[a] The fragments are $MO(H_2O)_p^{2+}$ and CH_4.

what would be obtained in water solvent. This difference between gas phase and solvent has been observed in Car−Parrinello MD simulations on the FeO^{2+} catalyzed oxidation of methane to methanol in water solution.[25] It was found that the solvent effect raises the barrier by more than 80 kJ/mol. This explains that the methane to methanol conversion is not readily effected by ironoxo based catalysts or enzymes, even though the barrier in the gas phase is quite low. The solvent effect has also been studied with polarizable continuum models and a full explanation has been given[44] based on the very electronic structure characteristics of this reaction we are discussing in this work. The solvent effects will affect all the reactions similarly, and we therefore can use the present gas phase studies to obtain insight in the differences between the various metaloxo species.

V, Cr, Mn. For the earlier metal complexes (V, Cr, Mn), the high spin state surface lies above the low spin state surface in the entrance channel (before **TS1**) of the considered reaction (see Figure 10). In the vanadium case, the spin crossing occurs in the entrance channel of the second step (the rebound step). For the chromium complex, the high spin surface does not exhibit any intermediate **I** such as $[CrOH(H_2O)_5^{2+}, {}^{\bullet}CH_3]$. Thus, it is hard to predict when the spin crossing is likely to occur. In the manganese case, the spin crossing is likely to occur in the exit channel of the first step (the H-abstraction step).

Whereas the rebound step is, as observed before, an almost barrierless process in each case (see Table 6), the H-abstraction can exhibit quite a high barrier $\Delta E_{TS1}^{\ddagger}$, depending on the metal used (up to 198.9 kJ/mol in the vanadium case, see Table 7). For the H-abstraction step, the energetic cost ΔE_1 *and* the energy barrier $\Delta E_{TS1}^{\ddagger}$ decrease along the series V, Cr, Mn. As one could expect, the lower the activation energy barrier is, the longer the O−H bond is (from 1.04 Å to 1.20 Å) and the shorter the C−H bond is (from 1.76 Å to 1.34 Å). The manganese complex is particularly efficient with a low energy barrier of 9.7 kJ/mol.

Let us then focus on the correlation between the electronic structure and the H-abstraction step efficiency. As we noticed previously, the $2\pi^*(\alpha)$ orbital is the lowest vacant acceptor orbital in this first group (V, Cr, Mn). According to the fragment analysis, the $\sigma(\alpha)_{C-H}$ donates electronic density to the $2\pi^*(\alpha)(MO^{2+})$ during the H-abstraction step (see Table 8). Indeed, in the transition state **TS1**, the $\sigma(\alpha)$(C−H) gross population has dropped from 1.00 in free CH_4 to 0.28 in **TS1**(V), 0.46 in **TS1**(Cr), 0.43 in **TS1**(Mn). Meanwhile, the $2\pi^*(\alpha)(MO^{2+})$ gross population has increased: from 0 in the free vanadium complex to 0.83 (0.40 + 0.43) in the transition state; from 0 in the free chromium complex to 1.66 (0.99 + 0.67) in the transition state; from 0 in the free Mn complex to 0.70 (0.74 − 0.04) in the transition state. In the Cr case, the transfer of 1.66 el. to the two $2\pi^*(\alpha)$ orbitals gives the impression of a two-electron transfer. However, this is not consistent with the decrease in population of the $\sigma(\alpha)_{C-H}$ orbital of −0.54. This apparent inconsistency is resolved if one takes into account that there is an electronic configuration change of the metal complex when going to the transition state: the $\delta_{x^2-y^2}(\alpha)$ is emptied in favor of the $2\pi^*(\alpha)$ orbital.

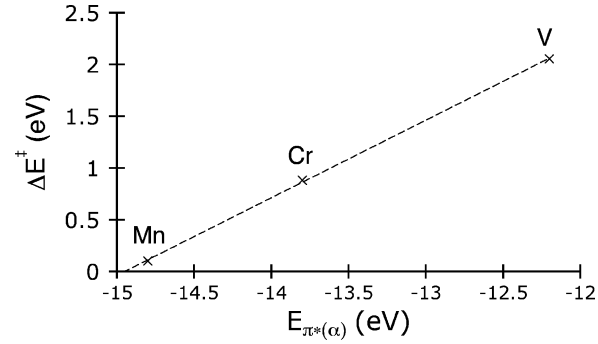

Figure 13. Activation energy of the H-abstraction step $\Delta E^{\ddagger}$ is linearly correlated to the energy of the lowest vacant molecular orbital ($E_{\pi^*(\alpha)}$) along the series $MO(H_2O)_5^{2+}$, M = V, Cr, Mn.

This electronic donation clearly controls the transition state geometry and the activation energy $\Delta E_{TS1}^{\ddagger}$. First, the transition state geometry presents an MOH angle of around 125° (see Table 7) which results from the balance between the orbital interaction (maximized for a 90° MOH angle) and the Pauli repulsion resulting from the equatorial water ligands, which increases when this angle approaches 90°. Then, at these angles of about 125° the activation energy $\Delta E_{TS1}^{\ddagger}$ is linearly correlated to the $2\pi^*(\alpha)$ orbital energy $\varepsilon_{\pi^*(\alpha)}$: $\Delta E_{TS1}^{\ddagger} = 0.75 \times \varepsilon_{\pi^*(\alpha)} + 11.212$ (in eV), with $R^2 = 0.9997$ (see Figure 13). So, the lower the $2\pi^*(\alpha)$ (MO^{2+}) lies in energy ($\varepsilon_{\pi^*(\alpha)}$), the lower the H-abstraction energy barrier ($\Delta E_{TS1}^{\ddagger}$) is.

Fe, Co. No spin crossing occurs during the C−H bond hydroxylation within this group. The reaction occurs on the high spin surface when catalyzed by $FeO(H_2O)_5^{2+}$ complex whereas it occurs on the low spin surface when catalyzed by $CoO(H_2O)_5^{2+}$ complex (see Figure 11).

This second group (Fe, Co) exhibits a $\sigma^*(\alpha)$ orbital as the lowest vacant acceptor orbital. From the fragment analysis, there is clearly an electronic donation from the $\sigma(\alpha)_{C-H}$ molecular orbital to the lowest $\sigma^*(\alpha)_{complex}$ molecular orbital during the H-abstraction (see Table 8): in the transition state structure, about half-electron has been donated from the $\sigma(\alpha)_{C-H}$ to the $\sigma^*(\alpha)_{complex}$. There is also a smaller donation from the $\sigma(\beta)_{C-H}$ molecular orbital to the lowest $\sigma^*(\beta)_{complex}$ molecular orbital (about 0.1 electron).

This donation clearly controls the transition state geometry: Pauli repulsion and orbital interaction are both in favor of a linear transition state (MOH angle around 180°). The $3\sigma^*(\alpha)$

(44) Louwerse, M.; Baerends, E. J. *Phys. Chem. Chem. Phys.* **2007**, 156.

lies lower in energy in the cobalt case than in the iron case (−14.5 eV vs −13.9 eV). The energy barriers ($\Delta E^{\ddagger}_{TS1}$) are close (11.7 kJ/mol vs 9.2 kJ/mol). Furthermore, if one compares with the first group (V, Cr, Mn), the energy barrier $\Delta E^{\ddagger}_{TS1}$ is particularly low given that the lowest acceptor orbital energies for, for example, the Cr and Mn complexes, are close to those of the Fe and Co complexes. For instance, the iron complex lowest vacant acceptor orbital energy (−13.9) is very close to the chromium complex one (−13.8 eV) whereas the energy barrier $\Delta E^{\ddagger}_{TS1}$ is much lower: 9.2 kJ/mol versus 84.9 kJ/mol. This huge difference in oxidative capability for a given lowest vacant orbital energy results from the difference in the nature of the lowest vacant orbital. In the chromium case, it is a $2\pi^*$ orbital whereas in the iron case, it is a $3\sigma^*$. During the electronic donation from the C−H bond into this lowest vacant acceptor orbital, the orbital interaction competes with the Pauli repulsion resulting from the water ligands. In both cases, the Pauli repulsion is minimized for an 180° angle whereas the orbital interaction stabilization is optimal for an angle of 90° in the chromium case and 180° in the iron case. The synergy between the strong orbital interaction stabilization and a reduced Pauli repulsion leads to an highly efficient iron complex whereas the disfavorable competition between those two terms leads to a less efficient chromium complex. So, the efficiency of the high spin FeO^{2+} arises from the energy and the orientation of the acceptor orbital, the $3\sigma^*(\alpha)$. According to this study, the high spin CoO^{2+} should be as efficient as the high spin FeO^{2+}, exhibiting the same acceptor orbital.

Ni, Cu. For these late metal complexes, the high spin surface lies below the low spin surface in the entrance channel of the oxidative process (see Figure 12). Then, this high spin state is highly destabilized once the H-abstraction has been carried out: no structure could be optimized for the intermediate species **PC** ($MCH_3OH(H_2O)_4^{2+}$). On the other hand, the low spin surface is highly reactive in both cases. It lies much higher in energy than the high spin surface. The reactant complex **RC** is even higher in energy than the isolated molecules. However, once the CH_4−O distance is small enough (<3 Å), the oxidation of the C−H bond occurs without any barrier, yielding the very stable species $MCH_3OH(H_2O)_4^{2+}$. As a consequence, the spin crossing occurs necessarily before the rebound step, but it is hard to say when exactly.

Let us focus now on the high spin surface reactivity. Let us remember that this last group (Ni, Cu) is characterized first by a different coordination environment, four water molecules instead of five, and second by a $\pi^*(\beta)$ orbital as the lowest vacant acceptor orbital. Once again, the fragment analysis demonstrates that the lowest acceptor orbitals, namely, here the $\pi^*(\beta)$ orbitals, accept electronic density from the $\sigma_{C-H}\beta$ orbital (around 0.6 electron, see Table 8). In this group, the donation from the $\sigma(\alpha)_{C-H}$ orbital to some acceptor molecular orbital of the complex is not feasible: all the α acceptor molecular orbitals are occupied.

The $\sigma_{C-H}\beta \rightarrow 2\pi^*_{x,y}\beta$ donation clearly controls the transition state geometry. Similarly to the V, Cr, Mn group, where also donation into $2\pi^*$ prevails, the **TS1** geometry presents an MOH angle of around 125° (see Table 7), resulting from the balance between orbital interaction (optimal for 90°) and Pauli repulsion (mimimal for 180°). Furthermore, this donation also controls the H-abstraction energy barrier ($\Delta E^{\ddagger}_{TS1}$): the lower the $2\pi^*(\beta)$ lies in energy, the lower $\Delta E^{\ddagger}_{TS1}$ is. But given the very low energy of the acceptor orbitals in this group, particularly in the Cu complex (−16.3 eV), one might have expected an even lower barrier than the low one we have obtained (14.5 kJ/mol for Ni, 6.8 kJ/mol for Cu), or even a barrierless process. An explanation may be the larger Pauli repulsion due to all the occupied α orbitals of the metal complex. Nevertheless, if such species could be generated, they would be highly reactive.

Summary: π^* versus σ^* Control along the Series. The MO^{2+} electrophilicity can be quantified through the H-abstraction energy barrier: the lower $\Delta E^{\ddagger}_{TS1}$ is, the more electrophilic the MO^{2+} moiety is. We have seen previously that the H-abstraction step can be controlled by the electron donation from the σ_{C-H} orbital into the lowest vacant acceptor orbital, namely, the lowest $2\pi^*$ or the $3\sigma^*(\alpha)$. In the first and the last group (V, Cr, Mn and Ni, Cu), the MO^{2+} electrophilicity is under $2\pi^*$ control whereas in the Fe and Co cases, the MO^{2+} electrophilicity is under $3\sigma^*(\alpha)$ control. Let us analyze further the differences between $2\pi^*$ and $3\sigma^*(\alpha)$ control.

Under the $2\pi^*$ control, the lower the $2\pi^*$ orbital lies in energy, the more electrophilic the MO^{2+} moiety is. In the first group, $\varepsilon_{2\pi^*(\alpha)}$ and $\Delta E^{\ddagger}_{TS1}$ are even linearly correlated (see Figure 13). In the last group, the MO^{2+} electrophilicity is controlled by the $2\pi^*(\beta)$: the lower it is, the lower the H-abstraction barrier is. Given the low $2\pi^*(\beta)$ energy $\varepsilon_{2\pi^*(\beta)}$ for the Ni and Cu complexes, the H-abstraction energy barrier $\Delta E^{\ddagger}_{TS1}$ is higher than one might have expected. However, as we have already seen, the α orbitals are fully occupied. Hence, the donation from the $\sigma(\alpha)_{C-H}$ orbital to some 3d-based α acceptor molecular orbital of the complex is not feasible. Futhermore, we can divide the Pauli repulsion into two terms: (1) the Pauli repulsion generated by the interaction of occupied substrate orbitals with MO^{2+} occupied molecular orbitals, and (2) the Pauli repulsion with the ligands. From the first group (V, Cr, Mn) to the last one (Ni, Cu), the first term is increased by the greater number of electrons on MO^{2+} whereas the second term is decreased (only 4 ligands instead of 5). From the energy barriers $\Delta E^{\ddagger}_{TS1}$ one would infer that the larger Pauli repulsion with the MO^{2+} electrons in the last group than in the first one outweighs the reduced Pauli repulsion with the ligands. To conclude, under $2\pi^*$ control, the electrophilicity is directly correlated to the $2\pi^*$ energy only for a given Pauli repulsion.

Under $3\sigma^*(\alpha)$ control, which applies in the case of the Fe and Co complexes, the low energy barrier (around 10 kJ/mol) is striking. The orbital energy of the lowest vacant acceptor orbital of the iron complex is pretty close to the one of the chromium complex, whereas the energy barrier

is quite different: 9.2 kJ/mol in the iron case versus 84.9 kJ/mol in the chromium case. If we would apply the correlation between activation energy $\Delta E^{\ddagger}_{TS1}$ and the controlling orbital energy as obtained in the first group (Figure 13), we would obtain an activation barrier of 75.8 kJ/mol instead of 9.2 kJ/mol in the iron case. This is also true for the cobalt complex: for the H-abstraction step we would obtain an activation barrier of 32.3 kJ/mol instead of 11.7 kJ/mol. Obviously, when the reaction is performed under $3\sigma^*(\alpha)$ control it is much more efficient. The σ^* controlled reactions present lower barriers than the π^* controlled reactions for a given orbital energy thanks to the combination of two effects: (1) the Pauli repulsion with the ligands is lower in the linear geometry, and (2) the orbital overlap is larger (see Table 9).

Conclusions

In this work, we have systematically studied the methane-to-methanol reaction catalyzed by the first row transition-metal complexes $MO(H_2O)_p^{2+}$. This reaction follows a rebound mechanism in two steps: (1) H-abstraction leading to a MOH^{2+} species, and (2) carbon radical collapse onto this species. The first step is the kinetic controlling step for all the studied complexes. The activation barrier and the transition state geometry of this H-abstraction step are directly correlated to the nature of lowest acceptor orbital. The main results are as follows: (1) the σ^* controlled H-abstraction reactions present linear transition states and π^* controlled H-abstraction reactions present bent transition states, (2) the σ^* controlled reactions present lower activation barriers than the π^* controlled reactions for a given lowest acceptor orbital energy, and (3) the activation barrier is directly correlated to the lowest vacant orbital energy provided the Pauli repulsion remains the same (same number of ligands, similar number of electrons) and provided the lowest acceptor orbital remains of the same type (σ^* or π^*). So, now we can answer the question raised in the Introduction. Iron is so special because of the nature of its lowest acceptor orbital: a low lying $3\sigma^*(\alpha)$, which is particularly efficient in promoting the H-abstraction step according to our results. However, the Fe complex does not emerge from this study as the only one. According to our results, the cobalt complex should be as efficient as iron for the Fenton chemistry under the proper experimental conditions. Indeed, cobalt-based compounds have already been used successfully in oxidation of cyclohexane[45−47] and even in decomposition of organic dyes.[48]

Finally, this study leads on to other questions. For instance, what is the ligand environment effect in the cobalt complex? We have seen in the introduction that a nitrogen equatorial environment induces a less favorable low spin state and less reactive species in the iron case. Preliminary tests on the cobalt system indicate the effect to be in the same direction, but Cobalt seems to be less sensitive to those environmental effects. The $CoO(NH_3)_5^{2+}$ complex is high spin (quartet). Its lowest acceptor orbital is still the $3\sigma^*(\alpha)$($\varepsilon_{3\sigma^*(\alpha)} = -12.4$ eV). The H-abstraction step energy barrier is still quite low ($\Delta E_1^{\dagger} = 77.1$ kJ/mol), though much higher than for $CoO(H_2O)_5^{2+}$ (11.7 kJ/mol).

Another question concerns the charge effect. Let us take two isoelectronic complexes: $FeO(H_2O)_5^{2+}$ and $MnO(H_2O)_5^{+}$. The electronic structures of those two complexes are very similar: same spin state (quintet), same lowest acceptor orbital ($3\ \sigma^*(\alpha)$). However, the charge decrease from the Fe to the Mn complex induces orbitals lying higher in energy: $\varepsilon_{3\sigma^*(\alpha)}$ ($FeO(H_2O)_5^{2+}$) $= -13.9$ eV and $\varepsilon_{3\sigma^*(\alpha)}$ ($MnO(H_2O)_5^{+}$) $= -6.7$ eV. As expected, the activation barrier of the H-abstraction step catalyzed by $MnO(H_2O)_5^{+}$ is much higher than the one catalyzed by $FeO(H_2O)_5^{2+}$ ($\Delta E_1^{\dagger}$ (Mn) $= 105.3$ kJ/mol vs $\Delta E_1^{\dagger}$ (Fe) $= 9.2$ kJ/mol. The late transition metal complexes should be less sensitive to this charge effect. Indeed, with a lowest acceptor orbital lying at -9.7 eV, the $CuO(H_2O)_3^{+}$ complex seems to be a promising active species. CuO^{+} has already been postulated in some enzymes and biologically relevant systems as an possible intermediate.[49,50] These and other points will be the subject of further investigations.

Acknowledgment. Support by the National Research School Combination "Catalysis by Design" is gratefully acknowledged.

IC802095M

(45) Pokutsa, A. P.; Sheparovich, R. B.; Zaborovskii, A. B.; Kopylets, V. I. *Kinet. Catal.* **2002**, *43*, 691–697.
(46) Pokutsa, A. P.; Zaborovskii, A. B.; Sheparovich, R. B.; Kopylets, V. I.; Maksim-Lutsik, D. S. *Kinet. Catal.* **2003**, *44*, 121–128.
(47) Tong, J.; Zhen, L.; Xia, C. *J. Mol. Catal. A: Chem.* **2005**, *231*, 197–203.
(48) Chen, W. X.; Lu, W. Y.; Yao, Y. Y.; Xu, M. H. *Environ. Sci. Technol.* **2007**, *41*, 6240–6245.
(49) Kamachi, T.; Kihara, N.; Shiota, Y.; Yoshizawa, K. *Inorg. Chem.* **2005**, *44*, 4226–4236.
(50) Pitié, M.; Boldron, C.; Pratviel, G. *Adv. Inorg. Chem.* **2006**, *58*, 77–1330.